

# Spline Autoregression Method for Estimation of Quantile Spectrum

Ta-Hsin Li\*

January 3, 2025

## Abstract

The quantile spectrum was introduced in Li (2012; 2014) as an alternative tool for spectral analysis of time series. It has the capability of providing a richer view of time series data than that offered by the ordinary spectrum especially for nonlinear dynamics such as stochastic volatility. A novel method, called spline autoregression (SAR), is proposed in this paper for estimating the quantile spectrum as a bivariate function of frequency and quantile level, under the assumption that the quantile spectrum varies smoothly with the quantile level. The SAR method is facilitated by the quantile discrete Fourier transform (QDFT) based on trigonometric quantile regression. It is enabled by the resulting time-domain quantile series (QSER) which represents properly scaled oscillatory characteristics of the original time series around a quantile. A functional autoregressive (AR) model is fitted to the QSER on a grid of quantile levels by penalized least-squares with the AR coefficients represented as smoothing splines of the quantile level. While the ordinary AR model is widely used for conventional spectral estimation, the proposed SAR method provides an effective way of estimating the quantile spectrum as a bivariate function in comparison with the alternatives. This is confirmed by a simulation study.

*Keywords:* Fourier transform, quantile-frequency analysis, periodogram, quantile regression, smoothing spline, spectral analysis, time series

---

\*Formerly affiliated with IBM T. J. Watson Research Center. Email: THL024@OUTLOOK.COM

# 1 Introduction

Consider  $m$  stationary time series  $\{y_{j,t}\}$  ( $j = 1, \dots, m$ ) with continuous marginal probability distribution functions  $F_j(y) := \Pr\{y_{j,t} \leq y\}$  and probability density functions  $\dot{F}_j(y) > 0$ . Given a quantile level  $\alpha \in (0, 1)$ , let  $q_j(\alpha) := F_j^{-1}(\alpha)$  denote the  $\alpha$ -quantile of  $\{y_{j,t}\}$ , and given  $\tau \in \{0, \pm 1, \dots\}$ , let  $r_{jj'}(\tau, \alpha)$  denote the correlation coefficient between the level-crossing processes  $\{\mathcal{I}(y_{j,t} \leq q_j(\alpha))\}$  and  $\{\mathcal{I}(y_{j',t-\tau} \leq q_{j'}(\alpha))\}$ . Under the assumption that  $r_{jj'}(\tau, \alpha)$  is absolutely summable over  $\tau$  for all  $j, j' = 1, \dots, m$  and all  $\alpha \in (0, 1)$ , the quantile spectrum  $\mathbf{S}(\omega, \alpha) := [S_{jj'}(\omega, \alpha)]_{j,j'=1}^m$  in Li (2012; 2014) through trigonometric quantile regression can be expressed as

$$S_{jj'}(\omega, \alpha) := \eta_j(\alpha)\eta_{j'}(\alpha) \sum_{\tau=-\infty}^{\infty} r_{jj'}(\tau, \alpha) \exp(-i\omega\tau) \quad (0 \leq \omega < 2\pi), \quad (1)$$

where  $\eta_j(\alpha) := \sqrt{\alpha(1-\alpha)}\kappa_j(\alpha)$  and  $\kappa_j(\alpha) := 1/\dot{F}_j(q_j(\alpha))$ . It is easy to show that

$$\begin{aligned} r_{jj'}(\tau, \alpha) &= \frac{1}{\alpha(1-\alpha)} \{F_{jj',\tau}(q_j(\alpha), q_{j'}(\alpha)) - \alpha^2\} \\ &= 1 - \frac{1}{2\alpha(1-\alpha)} \gamma_{jj',\tau}(q_j(\alpha), q_{j'}(\alpha)), \end{aligned}$$

where  $F_{jj',\tau}(y, y') := \Pr\{y_{j,t} \leq y, y_{j',t-\tau} \leq y'\}$  denotes the distribution function of  $(y_{j,t}, y_{j',t-\tau})$ , and  $\gamma_{jj',\tau}(y, y') := \Pr\{(y_{j,t} - y)(y_{j',t-\tau} - y') < 0\}$  denotes the level-crossing rate of  $(y_{j,t}, y_{j',t-\tau})$ . Through these quantities, together with  $\eta_j(\alpha)$ , the quantile spectrum in (1), as a bivariate function of  $\omega$  and  $\alpha$ , provides a different and richer view of the time series than that offered by the conventional spectrum which is determined solely by the second-order moments.

Exploration of the quantile spectrum  $\mathbf{S}(\omega, \alpha)$  as a bivariate function of  $\omega$  and  $\alpha$  constitutes what we call quantile-frequency analysis or QFA (Li 2020; 2021). It contributes to a growing literature on nonlinear spectral analysis techniques (e.g., Kedem 1986; Hong 2000; Davis and Mikosch 2009; Hagemann 2013; Dette et al. 2015; Fajardo, et al. 2018; Baruník and Kley 2019; Meziani et al. 2020; Jordanger and Tjøstheim 2022; 2023; Lim and Oh 2022).

Unlike the conventional spectrum of level-crossing processes (e.g., Davis and Mikosch 2009; Hagemann 2013; Dette et al. 2015), the quantile spectrum defined by (1) retains the information about the marginal distribution through the scaling function  $\eta_j(\alpha)$  as a result of quantile regression. Furthermore, we treat the quantile spectrum  $\mathbf{S}(\omega, \alpha)$  as a bivariate function of  $\omega$  and  $\alpha$  rather than a univariate function of  $\omega$  for fixed  $\alpha$  as done typically in level-crossing-based techniques.

We focus on the situation in which  $\mathbf{S}(\omega, \alpha)$  varies smoothly with  $\alpha$ . We intend to leverage this smoothness to improve the estimation accuracy over the method that ignores the smoothness and estimates the spectrum independent at different quantiles.

The autoregressive (AR) model is widely used in conventional spectral analysis (Percival and Walden 1993; Stoica and Moses 1997). This AR approach has been extended to estimate the quantile spectrum in Chen et al. (2022) and Jiménez-Varón et al. (2024). In these works, an AR model is derived from the quantile periodogram at each quantile level in a finite grid, and the resulting AR parameters are smoothed nonparametrically across the quantile levels to produce a bivariate function of  $\omega$  and  $\alpha$  for estimating the quantile spectrum.

In this paper, we propose a new method that combines autoregression and quantile smoothing into a unified penalized-least-squares problem. This method, called spline autoregression (SAR), is enabled by what we call the quantile series (QSER). Each QSER is derived from the original time series through what we call the quantile discrete Fourier transform (QDFT) at a quantile level based on trigonometric quantile regression. This series presents properly scaled oscillatory characteristics of the original series around the corresponding quantile. The SAR method employs a functional AR model in which the parameters are spline functions of  $\alpha$ ; this model is fitted by penalized least-squares to the QSER on a finite grid of quantile levels, yielding a bivariate estimate of the quantile spectrum in which the parameters are smoothing splines of  $\alpha$ . A

simulation study shows that the SAR estimator is able to produce more accurate estimates than the alternatives which apply autoregression independently to the QSER at each quantile level with or without subsequent smoothing across quantiles.

The rest of the paper is organized as follows. Section 2 introduces the QDFT and the resulting quantile periodogram (QPER); Section 3 introduces the QSER and the SAR estimator. Section 4 discusses some properties of the SAR estimator. Section 5 presents the result of a simulation study that evaluates the proposed method. Concluding remarks are given in Section 6.

Supplementary material to the main body of the paper includes discussions on the computation of the SAR estimator and its application to Granger-causality analysis in Appendix I and II, additional simulation results in Appendix III, a summary of R functions that implement the proposed method in Appendix IV.

## 2 Quantile Fourier Transform and Quantile Periodogram

Given a data record  $\{y_{j,t} : t = 1, \dots, n\}$  ( $j = 1, \dots, m$ ), consider the quantile regression problem

$$\hat{\boldsymbol{\beta}}_j(\omega, \alpha) := \underset{\boldsymbol{\beta}}{\operatorname{argmin}} \sum_{t=1}^n \rho_\alpha(y_{j,t} - \mathbf{x}_t^T(\omega) \boldsymbol{\beta}), \quad (2)$$

where  $\omega \in [0, 2\pi)$  is the frequency variable,  $\alpha \in (0, 1)$  is the quantile level variable,  $\rho_\alpha(y) := y(\alpha - \mathcal{I}(y \leq 0))$  is the objective function of quantile regression (Koenker 2005, p. 5), and  $\mathbf{x}_t(\omega)$  is a trigonometric regressor defined by

$$\mathbf{x}_t(\omega) := \begin{cases} 1 & \omega = 0, \\ [1, \cos(\pi t)]^T & \omega = \pi, \\ [1, \cos(\omega t), \sin(\omega t)]^T & \text{otherwise.} \end{cases} \quad (3)$$

The solution of (2) takes the form

$$\hat{\boldsymbol{\beta}}_j(\omega, \alpha) = \begin{cases} \hat{\beta}_{1,j}(0, \alpha) & \omega = 0, \\ [\hat{\beta}_{1,j}(\pi, \alpha), \hat{\beta}_{2,j}(\pi, \alpha)]^T & \omega = \pi, \\ [\hat{\beta}_{1,j}(\omega, \alpha), \hat{\beta}_{2,j}(\omega, \alpha), \hat{\beta}_{3,j}(\omega, \alpha)]^T & \text{otherwise.} \end{cases} \quad (4)$$

Based on these quantities, we define

$$Z_j(\omega, \alpha) := \begin{cases} n\hat{\beta}_{1,j}(0, \alpha) & \omega = 0, \\ n\hat{\beta}_{2,j}(\pi, \alpha) & \omega = \pi, \\ (n/2)\{\hat{\beta}_{2,j}(\omega, \alpha) - i\hat{\beta}_{3,j}(\omega, \alpha)\} & \text{otherwise,} \end{cases} \quad (5)$$

where  $i := \sqrt{-1}$ . The quantile periodogram (QPER) introduced in Li (2012; 2014) can be expressed as  $\mathbf{Q}(\omega, \alpha) := [Q_{jj'}(\omega, \alpha)]_{j,j'=1}^m$ , where

$$Q_{jj'}(\omega, \alpha) := n^{-1}Z_j(\omega, \alpha)Z_{j'}^*(\omega, \alpha) \quad (j, j' = 1, \dots, m). \quad (6)$$

Under suitable conditions (Li 2014, p. 557), it can be shown that for any fixed  $0 < \lambda_1 < \dots < \lambda_q < \pi$ ,  $\mathbf{Q}(\lambda_1, \alpha), \dots, \mathbf{Q}(\lambda_q, \alpha)$  are asymptotically distributed as  $\boldsymbol{\zeta}_1 \boldsymbol{\zeta}_1^H, \dots, \boldsymbol{\zeta}_q \boldsymbol{\zeta}_q^H$ , where  $\boldsymbol{\zeta}_1, \dots, \boldsymbol{\zeta}_q$  are independent complex Gaussian random vectors with zero mean and covariance matrix  $\mathbf{S}(\lambda_1, \alpha), \dots, \mathbf{S}(\lambda_q, \alpha)$ , respectively. This is analogous to a property of the ordinary periodogram where  $\mathbf{S}(\omega, \alpha)$  plays the role of the ordinary spectrum (Brockwell and Davis 1991, p. 446).

Let  $\omega_v := 2\pi v/n$  ( $v = 0, 1, \dots, n-1$ ) be the  $n$  Fourier frequencies. For each  $j \in \{1, \dots, m\}$ , the sequence  $\{Z_j(\omega_v, \alpha) : v = 0, 1, \dots, n-1\}$  constitutes what we call the quantile discrete Fourier transform (QDFT) of  $\{y_{j,t} : t = 1, \dots, n\}$  at quantile level  $\alpha$  (Li 2022). The QDFT is an extension of the ordinary DFT,  $Z_j(\omega_v) := \sum_{t=1}^n y_{j,t} \exp(-i\omega_v t)$  ( $v = 0, \dots, n-1$ ), because the latter can be obtained from the same trigonometric regression machinery (2)–(6) with  $\rho_\alpha(y)$  replaced by  $y^2$ . Similarly, the quantile periodogram  $\{\mathbf{Q}(\omega_v, \alpha) : v = 0, 1, \dots, n-1\}$  is an extension of the ordinary periodogram  $\{[I_{jj'}(\omega_v)]_{j,j'=1}^m : v = 0, 1, \dots, n-1\}$ , where  $I_{jj'}(\omega_v) := n^{-1}Z_j(\omega_v)Z_{j'}^*(\omega_v)$ .

### 3 Quantile Series and Spline Autoregression Estimator

Associated with the QDFT is a time-domain series, which we call the quantile series (QSER), defined as the inverse discrete Fourier transform of the QDFT, i.e.,

$$y_{j,t}(\alpha) := n^{-1} \sum_{v=0}^{n-1} Z_j(\omega_v, \alpha) \exp(it\omega_v) \quad (t = 1, \dots, n). \quad (7)$$

This is a real-valued sequence with mean  $\bar{y}_j(\alpha) := n^{-1} \sum_{t=1}^n y_{j,t}(\alpha)$  equalling  $\hat{\beta}_j(0, \alpha)$ , the  $\alpha$ -quantile of  $\{y_{j,t} : t = 1, \dots, n\}$ . The quantile periodogram  $\{\mathbf{Q}(\omega_v, \alpha) : v = 0, 1, \dots, n-1\}$  coincides with the ordinary periodogram of  $\{y_{j,t}(\alpha) : t = 1, \dots, n\}$ . This observation gives rise to the idea of applying conventional spectral estimation techniques to the QSER in developing different estimators for the quantile spectrum.

This idea can be further justified by considering the quantile-crossing process

$$u_{j,t}(\alpha) := q_j(\alpha) + \kappa_j(\alpha) (\alpha - \mathcal{I}(y_{j,t} \leq q_j(\alpha))). \quad (8)$$

This process is stationary with mean  $q_j(\alpha)$  and variance  $\eta_j^2(\alpha)$ . Under suitable conditions (Wu 2007; Li 2012), we have the Bahadur-type representations

$$\begin{aligned} \hat{\beta}_{1,j}(0, \alpha) &= n^{-1} \sum_{t=1}^n u_{j,t}(\alpha) + o_P(n^{-1/2}), \\ \hat{\beta}_{2,j}(\pi, \alpha) &= n^{-1} \sum_{t=1}^n u_{j,t}(\alpha) \cos(\pi t) + o_P(n^{-1/2}), \\ \hat{\beta}_{2,j}(\omega_v, \alpha) &= 2n^{-1} \sum_{t=1}^n u_{j,t}(\alpha) \cos(\omega_v t) + o_P(n^{-1/2}) \quad \omega_v \notin \{0, \pi\}, \\ \hat{\beta}_{3,j}(\omega_v, \alpha) &= 2n^{-1} \sum_{t=1}^n u_{j,t}(\alpha) \sin(\omega_v t) + o_P(n^{-1/2}) \quad \omega_v \notin \{0, \pi\}. \end{aligned}$$

Therefore, it follows that

$$y_{j,t}(\alpha) = u_{j,t}(\alpha) + e_{j,t}(\alpha)$$

and  $n^{-1} \sum_{t=1}^n \{e_{j,t}(\alpha)\}^2 = o_P(1)$ . In other words, the QSER can be viewed as an approximation to the underlying quantile-crossing process whose ordinary spectrum coincides with  $\mathbf{S}(\omega, \alpha)$ .

Let  $\mathbf{\Gamma}(\tau, \alpha)$  denote the autocovariance function (ACF) of  $\mathbf{u}_t(\alpha) := [u_{1,t}(\alpha), \dots, u_{m,t}(\alpha)]^T$ .

Then, the quantile spectrum  $\mathbf{S}(\omega, \alpha)$  can be expressed as

$$\mathbf{S}(\omega, \alpha) = \sum_{\tau=-\infty}^{\infty} \mathbf{\Gamma}(\tau, \alpha) \exp(-i\omega\tau).$$

This relationship was exploited in Li (2022) to devise the lag-window (LW) estimator

$$\hat{\mathbf{S}}_{\text{LW}}(\omega, \alpha) = \sum_{|\tau| \leq M} h(\tau/M) \hat{\mathbf{\Gamma}}(\tau, \alpha) \exp(-i\omega\tau), \quad (9)$$

where  $h(\cdot)$  is a window function and  $\hat{\mathbf{\Gamma}}(\tau, \alpha)$  is the ACF of  $\{y_{j,t}(\alpha) : t = 1, \dots, n\}$  ( $j = 1, \dots, m$ ), called the quantile ACF (QACF), which serves as an estimate of  $\mathbf{\Gamma}(\tau, \alpha)$ .

In the following, we focus on the AR approach. Let  $\mathbf{A}_p(\alpha) := [\mathbf{A}_{p,1}(\alpha), \dots, \mathbf{A}_{p,p}(\alpha)]$  denote the matrix of AR coefficients obtained from the Yule-Walker equations of an AR( $p$ ) process whose ACF is  $\mathbf{\Gamma}(\tau, \alpha)$  ( $\tau = 0, \pm 1, \dots$ ), and let  $\mathbf{V}_p(\alpha) := [\sigma_{jj'}(\alpha)]_{j,j'=1}^m$  denote the resulting residual covariance matrix. It can be shown (Lütkepohl 1993, p. 78) that

$$\mathbf{A}_p(\alpha) = \boldsymbol{\gamma}_p(\alpha) \mathbf{\Gamma}_p^{-1}(\alpha), \quad \mathbf{V}_p(\alpha) = \mathbf{\Gamma}(0, \alpha) - \mathbf{A}_p(\alpha) \boldsymbol{\gamma}_p^T(\alpha), \quad (10)$$

where  $\mathbf{\Gamma}_p(\alpha) := [\mathbf{\Gamma}(\tau - \tau', \alpha)]_{\tau, \tau'=1}^p$  and  $\boldsymbol{\gamma}_p(\alpha) := [\mathbf{\Gamma}(1, \alpha), \dots, \mathbf{\Gamma}(p, \alpha)]$ . Associated with these parameters is the AR spectrum

$$\mathbf{S}_p(\omega, \alpha) := (\mathbf{I} - \mathbf{A}_p(\omega, \alpha))^{-1} \mathbf{V}_p(\alpha) (\mathbf{I} - \mathbf{A}_p(\omega, \alpha))^{-H}, \quad (11)$$

with  $\mathbf{A}_p(\omega, \alpha) := \sum_{\tau=1}^p \mathbf{A}_{p,\tau} \exp(-i\omega\tau)$ . This spectrum has the maximum entropy property (Parzen 1982; Choi 1993), i.e., it maximizes the entropy among all spectra whose first  $p + 1$  autocovariances coincide with  $\{\mathbf{\Gamma}(\tau, \alpha) : \tau = 0, 1, \dots, p\}$ . We employ this spectrum as a model to approximate  $\mathbf{S}(\omega, \alpha)$ . The error of approximation satisfies

$$\|\mathbf{S}_p(\omega, \alpha) - \mathbf{S}(\omega, \alpha)\|_1 \leq \sum_{|\tau| > p} \|\mathbf{\Gamma}_p(\tau, \alpha)\|_1 + \sum_{|\tau| > p} \|\mathbf{\Gamma}(\tau, \alpha)\|_1, \quad (12)$$

where  $\mathbf{\Gamma}_p(\tau, \alpha)$  is the ACF of the AR model satisfying  $\mathbf{S}_p(\omega, \alpha) = \sum_{\tau=-\infty}^{\infty} \mathbf{\Gamma}_p(\tau, \alpha) \exp(-i\omega\tau)$ .

The second term on the right-hand side of (12) tends to zero as  $p \rightarrow \infty$ , due to the assumption

that all entries in  $\mathbf{\Gamma}(\tau, \alpha)$  are absolutely summable over  $\tau$ . If the first term also tends to zero, we would have  $\|\mathbf{S}_p(\omega, \alpha) - \mathbf{S}(\omega, \alpha)\|_1 \rightarrow 0$  as  $p \rightarrow \infty$ , which justifies the AR approach. Another way of justifying this approach is through the  $\text{AR}(\infty)$  representation of  $\mathbf{S}(\omega, \alpha)$  as the ordinary spectrum of  $\{\mathbf{u}_t(\alpha)\}$  (Wiener and Masani 1957; 1958; Whittle 1963).

For fixed  $\alpha$ , the AR parameters in (11) can be estimated by solving the Yule-Walker equations with  $\{\mathbf{\Gamma}(\tau, \alpha) : \tau = 0, 1, \dots, p\}$  replaced by  $\{\hat{\mathbf{\Gamma}}(\tau, \alpha) : \tau = 0, 1, \dots, p\}$ . To obtain an estimate over a given interval of  $\alpha \in [\underline{\alpha}, \bar{\alpha}] \subset (0, 1)$ , one may first compute the AR parameters for each quantile level in a finite grid  $\alpha_1 := \underline{\alpha} < \alpha_2 < \dots < \alpha_L := \bar{\alpha}$ , and then apply a smoothing procedure to the resulting AR parameters across the quantile levels  $\{\alpha_\ell : \ell = 1, \dots, L\}$ . This two-step method has been explored by Chen et al. (2022) and Jiménez-Varón et al. (2024) with  $\hat{\mathbf{\Gamma}}(\tau, \alpha)$  derived from the quantile periodogram instead of the QSER.

We propose a new method of estimating the AR parameters in (11) as functions of  $\alpha \in [\underline{\alpha}, \bar{\alpha}]$ . This method, called spline autoregression (SAR), is based on least-squares autoregression which is applied jointly to the QSER for all  $\alpha_\ell$  ( $\ell = 1, \dots, L$ ). The AR parameters in (11) are represented as spline functions of  $\alpha \in [\underline{\alpha}, \bar{\alpha}]$  and penalized for their roughness in the least-squares procedure.

More precisely, let  $\mathbf{y}_t(\alpha_\ell) := [y_{1,t}(\alpha_\ell) - \bar{y}_1(\alpha_\ell), \dots, y_{m,t}(\alpha_\ell) - \bar{y}_m(\alpha_\ell)]^T$  ( $t = 1, \dots, n$ ) denote the demeaned QSER at  $\alpha_\ell$  ( $\ell = 1, \dots, L$ ). Then, the SAR problem can be stated as

$$\begin{aligned} \{\hat{\mathbf{A}}_1(\cdot), \dots, \hat{\mathbf{A}}_p(\cdot)\} &:= \underset{\mathbf{A}_1(\cdot), \dots, \mathbf{A}_p(\cdot) \in \mathcal{F}_m}{\operatorname{argmin}} \sum_{\ell=1}^L (n-p)^{-1} \sum_{t=p+1}^n \left\| \mathbf{y}_t(\alpha_\ell) - \sum_{\tau=1}^p \mathbf{A}_\tau(\alpha_\ell) \mathbf{y}_{t-\tau}(\alpha_\ell) \right\|^2 \\ &\quad + \lambda \sum_{\tau=1}^p \int_{\underline{\alpha}}^{\bar{\alpha}} \|\ddot{\mathbf{A}}_\tau(\alpha)\|^2 d\alpha \end{aligned} \quad (13)$$

where  $\mathcal{F}_m$  is the space spanned by  $m$ -by- $m$  matrices of spline basis functions in  $[\underline{\alpha}, \bar{\alpha}]$  and  $\lambda > 0$  is the smoothing parameter that specifies the amount of penalty for the roughness of the functional AR coefficients as measured by the integral of the Frobenius norm of second derivative. In



addition, let the residual covariance matrix at  $\alpha_\ell$  be defined by

$$\begin{aligned}\tilde{\mathbf{V}}(\alpha_\ell) &:= [\tilde{\sigma}_{jj'}(\alpha_\ell)]_{j,j'=1}^m \\ &:= (n-p)^{-1} \sum_{t=p+1}^n \left[ \mathbf{y}_t(\alpha_\ell) - \sum_{\tau=1}^p \hat{\mathbf{A}}_\tau(\alpha_\ell) \mathbf{y}_{t-\tau}(\alpha_\ell) \right] \\ &\quad \times \left[ \mathbf{y}_t(\alpha_\ell) - \sum_{\tau=1}^p \hat{\mathbf{A}}_\tau(\alpha_\ell) \mathbf{y}_{t-\tau}(\alpha_\ell) \right]^T.\end{aligned}$$

Applying the smoothing spline technique to  $\{\tilde{\sigma}_{jj'}(\alpha_\ell) : \ell = 1, \dots, L\}$  yields

$$\hat{\mathbf{V}}(\cdot) := [\hat{\sigma}_{jj'}(\cdot)]_{j,j'=1}^m. \quad (14)$$

where

$$\hat{\sigma}_{jj'}(\cdot) := \operatorname{argmin}_{\sigma(\cdot) \in \mathcal{F}_1} \left\{ \sum_{\ell=1}^L (\tilde{\sigma}_{jj'}(\alpha_\ell) - \sigma(\alpha_\ell))^2 + \lambda \int_{\underline{\alpha}}^{\bar{\alpha}} (\ddot{\sigma}(\alpha))^2 d\alpha \right\}. \quad (15)$$

Note that we set the smoothing parameter in (15) to be identical to the smoothing parameter in (13) for consistency and simplicity, although it could take a different value  $\lambda_{jj'}$  in general.

The SAR solution given by (13)–(15) can be viewed as a smoothing spline estimate of the AR parameters  $\{\mathbf{A}_{p,1}(\cdot), \dots, \mathbf{A}_{p,p}(\cdot)\}$  and  $\mathbf{V}_p(\cdot)$  in (11) defined by the Yule-Walker equations. Plugging these estimates in (11) leads to the SAR spectral estimator

$$\hat{\mathbf{S}}(\omega, \alpha) := (\mathbf{I} - \hat{\mathbf{A}}(\omega, \alpha))^{-1} \hat{\mathbf{V}}(\alpha) (\mathbf{I} - \hat{\mathbf{A}}(\omega, \alpha))^{-H}, \quad (16)$$

where  $\hat{\mathbf{A}}(\omega, \alpha) := \mathbf{I} - \sum_{\tau=1}^p \hat{\mathbf{A}}_\tau(\alpha) \exp(-i\tau\omega)$  and  $(\omega, \alpha) \in [0, 2\pi) \times [\underline{\alpha}, \bar{\alpha}]$ .

To complete the procedure, we propose a data-driven method for selecting  $p$  and  $\lambda$  in (13): First, for each  $\ell = 1, \dots, L$ , fit an AR( $p$ ) model to  $\{\mathbf{y}_t(\alpha_\ell) : t = 1, \dots, n\}$  to obtain Akaike's information criterion  $\text{AIC}_p(\alpha_\ell)$  with  $p = 0, 1, \dots, p_0$  (Lütkepohl 1993, p. 129), where  $p_0$  is a pre-determined maximum order. Then, choose  $p$  to minimize the average AIC across the quantile levels, i.e.,  $L^{-1} \sum_{\ell=1}^L \text{AIC}_p(\alpha_\ell)$ . Finally, with  $p$  given and fixed, choose  $\lambda$  to minimize the generalized cross-validation (GCV) criterion

$$\text{GCV}(\lambda) := \frac{(L(n-p))^{-1} \sum_{\ell=1}^L \sum_{t=p+1}^n \|\mathbf{y}_t(\alpha_\ell) - \sum_{\tau=1}^p \hat{\mathbf{A}}_\tau(\alpha_\ell) \mathbf{y}_{t-\tau}(\alpha_\ell)\|^2}{\{1 - (L(n-p))^{-1} \text{tr}(\mathbf{H})\}^2}, \quad (17)$$

where  $\text{tr}(\mathbf{H})$  is the trace of the hat matrix associated with (13) (see Appendix I for details), which serves as the effective degree of freedom (Hastie and Tibshirani 1990, p. 52). Note that selecting  $\lambda$  and  $p$  jointly to minimize the GCV in (17) is problematic, because the response of  $\text{tr}(\mathbf{H})$  to over-parameterization with a large  $p$  can be mitigated by the choice of a large  $\lambda$ . The proposed method of selecting  $p$  independently before  $\lambda$  overcomes this difficulty.

## 4 Characterization of the Spline Autoregression Estimator

Let  $\{\phi_k(\cdot) : k = 1, \dots, K\}$  denote a set of spline basis functions on  $[\underline{\alpha}, \bar{\alpha}]$ . For any  $\mathbf{A}_\tau(\cdot) \in \mathcal{F}_m$ , there exists  $\Theta_\tau := [\Theta_{\tau,1}, \dots, \Theta_{\tau,K}] \in \mathbb{R}^{m \times Km}$  such that

$$\mathbf{A}_\tau(\cdot) := \sum_{k=1}^K \Theta_{\tau,k} \phi_k(\cdot) = \Theta_\tau \Phi(\cdot),$$

where  $\Phi(\cdot) := [\phi_1(\cdot)\mathbf{I}_m, \dots, \phi_K(\cdot)\mathbf{I}_m]^T \in \mathbb{R}^{Km \times m}$ . Define

$$\begin{aligned} \mathbf{Y}_\ell &:= [\mathbf{y}_{p+1}(\alpha_\ell), \dots, \mathbf{y}_n(\alpha_\ell)] \in \mathbb{R}^{m \times (n-p)}, \\ \mathbf{Z}_\ell &:= \begin{bmatrix} \Phi(\alpha_\ell) \mathbf{y}_p(\alpha_\ell) & \cdots & \Phi(\alpha_\ell) \mathbf{y}_{n-1}(\alpha_\ell) \\ \vdots & & \vdots \\ \Phi(\alpha_\ell) \mathbf{y}_1(\alpha_\ell) & \cdots & \Phi(\alpha_\ell) \mathbf{y}_{n-p}(\alpha_\ell) \end{bmatrix} \in \mathbb{R}^{Kmp \times (n-p)}, \\ \mathbf{D} &:= \mathbf{I}_p \otimes \int_{\underline{\alpha}}^{\bar{\alpha}} \Phi(\alpha) \Phi^T(\alpha) d\alpha \in \mathbb{R}^{Kmp \times Kmp}. \end{aligned}$$

With this notation, we have the following results for the SAR solution in (13).

**Proposition 1.** (a) The solution of (13) can be expressed as

$$\hat{\mathbf{A}}(\cdot) := [\hat{\mathbf{A}}_1(\cdot), \dots, \hat{\mathbf{A}}_p(\cdot)] = [\hat{\Theta}_1 \Phi(\cdot), \dots, \hat{\Theta}_p \Phi(\cdot)] = \hat{\Theta} (\mathbf{I}_p \otimes \Phi(\cdot)),$$

where

$$\hat{\Theta} := [\hat{\Theta}_1, \dots, \hat{\Theta}_p] := \left( \sum_{\ell=1}^L \mathbf{Y}_\ell \mathbf{Z}_\ell^T \right) \left( \sum_{\ell=1}^L \mathbf{Z}_\ell \mathbf{Z}_\ell^T + (n-p)\lambda \mathbf{D} \right)^{-1}. \quad (18)$$

(b) As  $n \rightarrow \infty$ , if  $\hat{\Gamma}(\tau, \alpha) \xrightarrow{P} \Gamma(\tau, \alpha)$  for any fixed  $\tau$  and  $\alpha$ , then  $\hat{\mathbf{A}}(\alpha) \xrightarrow{P} \bar{\mathbf{A}}(\alpha) := \bar{\Theta}(\mathbf{I}_p \otimes \Phi(\alpha))$  uniformly in  $\alpha \in [\underline{\alpha}, \bar{\alpha}]$ , where

$$\begin{aligned} \bar{\Theta} &:= \left( \sum_{\ell=1}^L \mathbf{A}_p(\alpha_\ell) \Gamma_p(\alpha_\ell) (\mathbf{I}_p \otimes \Phi^T(\alpha_\ell)) \right) \\ &\quad \times \left( \sum_{\ell=1}^L (\mathbf{I}_p \otimes \Phi(\alpha_\ell)) \Gamma_p(\alpha_\ell) (\mathbf{I}_p \otimes \Phi^T(\alpha_\ell) + \lambda \mathbf{D}) \right)^{-1}. \end{aligned}$$

(c) If  $\mathbf{A}_{p,\tau}(\cdot) \in \mathcal{F}_m$  for all  $\tau = 1, \dots, p$ , then, as  $\lambda \rightarrow 0$ ,  $\bar{\mathbf{A}}(\alpha) \rightarrow \mathbf{A}_p(\alpha)$  uniformly in  $\alpha \in [\underline{\alpha}, \bar{\alpha}]$ .

PROOF: The proof of assertion (a) can be found in Appendix I. To prove assertion (b), we note that  $\hat{\Gamma}(\tau, \alpha) \xrightarrow{P} \Gamma(\tau, \alpha)$  implies

$$\begin{aligned} (n-p)^{-1} \mathbf{Z}_\ell \mathbf{Z}_\ell^T &\xrightarrow{P} [\Phi(\alpha_\ell) \Gamma(\tau - \tau', \alpha_\ell) \Phi^T(\alpha_\ell)]_{\tau, \tau'=1}^p \\ &= (\mathbf{I}_p \otimes \Phi(\alpha_\ell)) \Gamma_p(\alpha_\ell) (\mathbf{I}_p \otimes \Phi^T(\alpha_\ell)), \\ (n-p)^{-1} \mathbf{Y}_\ell \mathbf{Z}_\ell^T &\xrightarrow{P} [\Gamma(1, \alpha_\ell) \Phi^T(\alpha_\ell), \dots, \Gamma(p, \alpha_\ell) \Phi^T(\alpha_\ell)] \\ &= \boldsymbol{\gamma}_p(\alpha_\ell) (\mathbf{I}_p \otimes \Phi^T(\alpha_\ell)). \end{aligned}$$

Combining this with (10) and (18) proves  $\hat{\Theta} \xrightarrow{P} \bar{\Theta}$ . Hence the assertion (b). Under the condition in (c), there exists  $\Theta \in \mathbb{R}^{m \times Kmp}$  such that  $\mathbf{A}_p(\cdot) = \Theta(\mathbf{I}_p \otimes \Phi(\cdot))$ . In this case,

$$\begin{aligned} \bar{\Theta} &= \Theta \left( \sum_{\ell=1}^L (\mathbf{I}_p \otimes \Phi(\alpha_\ell)) \Gamma_p(\alpha_\ell) (\mathbf{I}_p \otimes \Phi^T(\alpha_\ell)) \right) \\ &\quad \times \left( \sum_{\ell=1}^L (\mathbf{I}_p \otimes \Phi(\alpha_\ell)) \Gamma_p(\alpha_\ell) (\mathbf{I}_p \otimes \Phi^T(\alpha_\ell) + \lambda \mathbf{D}) \right)^{-1}. \end{aligned}$$

As  $\lambda \rightarrow 0$ , we have  $\bar{\Theta} \rightarrow \Theta$ . Therefore,  $\bar{\mathbf{A}}(\alpha) \rightarrow \Theta(\mathbf{I}_p \otimes \Phi(\alpha))$  uniformly in  $\alpha \in [\underline{\alpha}, \bar{\alpha}]$ .  $\square$

Similarly, the following results can be obtained for  $\hat{\mathbf{V}}(\cdot)$  in (14) with the notation  $\boldsymbol{\phi}(\alpha) := [\phi_1(\alpha), \dots, \phi_K(\alpha)]^T$ ,  $\mathbf{B} := [\boldsymbol{\phi}(\alpha_1), \dots, \boldsymbol{\phi}(\alpha_L)]^T$ , and  $\boldsymbol{\Omega} := \int_{\underline{\alpha}}^{\bar{\alpha}} \ddot{\boldsymbol{\phi}}(\alpha) \ddot{\boldsymbol{\phi}}^T(\alpha) d\alpha$ .

**Proposition 2.** (a) The solution of (15) can be expressed as  $\hat{\sigma}_{jj'}(\cdot) = \boldsymbol{\phi}^T(\cdot) \hat{\boldsymbol{\xi}}_{jj'}$ , where

$$\hat{\boldsymbol{\xi}}_{jj'} := (\mathbf{B}^T \mathbf{B} + \lambda \boldsymbol{\Omega})^{-1} \mathbf{B}^T \hat{\boldsymbol{\rho}}_{jj'}$$

and  $\hat{\boldsymbol{\rho}}_{jj'} := [\hat{\sigma}_{jj'}(\alpha_1), \dots, \hat{\sigma}_{jj'}(\alpha_L)]^T$ .

- (b) As  $n \rightarrow \infty$ , if  $\hat{\Gamma}(\tau, \alpha) \xrightarrow{P} \Gamma(\tau, \alpha)$  for any fixed  $\tau$  and  $\alpha$ , then  $\hat{\mathbf{V}}(\alpha) \xrightarrow{P} \bar{\mathbf{V}}(\alpha) := [\bar{\sigma}_{jj'}(\alpha)]_{j,j'=1}^m$  uniformly in  $\alpha \in [\underline{\alpha}, \bar{\alpha}]$ , where  $\bar{\sigma}_{jj'}(\alpha) := \boldsymbol{\phi}^T(\alpha) \bar{\boldsymbol{\xi}}_{jj'}$  and  $\bar{\boldsymbol{\xi}}_{jj'} := (\mathbf{B}^T \mathbf{B} + \lambda \boldsymbol{\Omega})^{-1} \mathbf{B}^T \bar{\boldsymbol{\rho}}_{jj'}$ , with  $\bar{\boldsymbol{\rho}}_{jj'}$  being the vector made of the  $(j, j')$ -th entry of

$$\boldsymbol{\Sigma}(\alpha_\ell) := \boldsymbol{\Gamma}(0, \alpha_\ell) - \bar{\mathbf{A}}(\alpha_\ell) \boldsymbol{\gamma}_p^T(\alpha_\ell) - \boldsymbol{\gamma}_p(\alpha_\ell) \bar{\mathbf{A}}^T(\alpha_\ell) + \bar{\mathbf{A}}(\alpha_\ell) \boldsymbol{\Gamma}_p(\alpha_\ell) \bar{\mathbf{A}}^T(\alpha_\ell)$$

for  $\ell = 1, \dots, L$ .

- (c) If  $\mathbf{A}_{p,\tau}(\cdot) \in \mathcal{F}_m$  for all  $\tau = 1, \dots, p$  and  $\mathbf{V}_p(\cdot) \in \mathcal{F}_m$ , then, as  $\lambda \rightarrow 0$ ,  $\bar{\mathbf{V}}_p(\alpha) \rightarrow \mathbf{V}_p(\alpha)$  uniformly in  $\alpha \in [\underline{\alpha}, \bar{\alpha}]$ .

PROOF: Assertion (a) is the standard result from spline smoothing (Hastie and Tibshirani 1990, p. 28). To prove assertion (b), observe that  $\tilde{\mathbf{V}}(\alpha_\ell) := [\tilde{\sigma}_{jj'}(\alpha_\ell)]_{j,j'=1}^m = (n-p)^{-1} \|\mathbf{Y}_\ell - \hat{\boldsymbol{\Theta}} \mathbf{Z}_\ell\|^2$ . Combining this expression with Proposition 1(b) yields  $\tilde{\mathbf{V}}(\alpha_\ell) \xrightarrow{P} \boldsymbol{\Sigma}(\alpha_\ell)$ . This implies that  $\hat{\boldsymbol{\rho}}_{jj'} \xrightarrow{P} \bar{\boldsymbol{\rho}}_{jj'}$ . Hence the assertion (b). Under the condition of (c),  $\bar{\mathbf{A}}(\alpha_\ell) \rightarrow \mathbf{A}_p(\alpha_\ell) = \boldsymbol{\gamma}_p(\alpha_\ell) \boldsymbol{\Gamma}_p^{-1}(\alpha_\ell)$  by Proposition 1(b). Therefore,  $\boldsymbol{\Sigma}(\alpha_\ell) \rightarrow \boldsymbol{\Gamma}(0, \alpha_\ell) - \mathbf{A}_p(\alpha_\ell) \boldsymbol{\gamma}_p^T(\alpha_\ell) = \mathbf{V}_p(\alpha_\ell)$ . This implies that  $\bar{\boldsymbol{\rho}}_{jj'} \rightarrow \boldsymbol{\rho}_{jj'}$ , where  $\boldsymbol{\rho}_{jj'}$  is the vector made of the  $(j, j')$ -th entry of  $\mathbf{V}_p(\alpha_\ell)$  for  $\ell = 1, \dots, L$ . If  $\mathbf{V}_p(\cdot) \in \mathcal{F}_m$ , then  $\sigma_{jj'}(\alpha) = \boldsymbol{\phi}^T(\alpha)$  for some  $\boldsymbol{\xi}_{jj'} \in \mathbb{R}^K$ . This implies that  $\boldsymbol{\rho}_{jj'} = \mathbf{B} \boldsymbol{\xi}_{jj'}$ . In this case,  $\bar{\boldsymbol{\xi}}_{jj'} \rightarrow \boldsymbol{\xi}_{jj'}$  and hence  $\bar{\sigma}_{jj'}(\alpha) \rightarrow \boldsymbol{\phi}^T(\alpha) \boldsymbol{\xi}_{jj'} = \sigma_{jj'}(\alpha)$  uniformly in  $\alpha \in [\underline{\alpha}, \bar{\alpha}]$ .  $\square$

By following the way  $\mathbf{S}_p(\omega, \alpha)$  in (11) is defined by the Yule-Walker solutions  $\mathbf{A}_p(\cdot)$  and  $\mathbf{V}_p(\cdot)$ , let  $\bar{\mathbf{S}}_p(\omega, \alpha)$  denote the spectrum defined by  $\bar{\mathbf{A}}_p(\cdot)$  and  $\bar{\mathbf{V}}_p(\cdot)$  in Propositions 1 and 2. In light of the above analysis,  $\bar{\mathbf{S}}_p(\omega, \alpha)$  can be viewed as a regularized version of  $\mathbf{S}_p(\omega, \alpha)$  based on smoothing spline parameters in  $\mathcal{F}_m$ . As an immediate result of Propositions 1 and 2, the following theorem summarizes the relations between these spectra and the SAR estimator  $\hat{\mathbf{S}}(\omega, \alpha)$  in (16).

**Theorem.** If  $\hat{\Gamma}(\tau, \alpha) \xrightarrow{P} \Gamma(\tau, \alpha)$  as  $n \rightarrow \infty$  for fixed  $\tau$  and  $\alpha$ , then  $\hat{\mathbf{S}}(\omega, \alpha) \xrightarrow{P} \bar{\mathbf{S}}_p(\omega, \alpha)$  uniformly in  $(\omega, \alpha) \in [0, 2\pi) \times [\underline{\alpha}, \bar{\alpha}]$ . In addition, if the AR parameters in (11) are members of  $\mathcal{F}_m$ , then  $\bar{\mathbf{S}}_p(\omega, \alpha) \rightarrow \mathbf{S}_p(\omega, \alpha)$  as  $\lambda \rightarrow 0$  uniformly in  $(\omega, \alpha) \in [0, 2\pi) \times [\underline{\alpha}, \bar{\alpha}]$ .

## 5 Simulation Study

To evaluate the SAR estimator, we present the results of a simulation study using a set of simulated data with  $m = 2$ . Additional results can be found in Appendix III.

Let  $\{\xi_{1,t}\}$ ,  $\{\xi_{2,t}\}$ , and  $\{\xi_{3,t}\}$  be zero-mean and unit-variance AR series satisfying  $\xi_{1,t} = a_{11} \xi_{1,t-1} + \varepsilon_{1,t}$ ,  $\xi_{2,t} = a_{21} \xi_{2,t-1} + \varepsilon_{2,t}$ , and  $\xi_{3,t} = a_{31} \xi_{3,t-1} + a_{32} \xi_{3,t-2} + \varepsilon_{3,t}$ , where  $a_{11} := 0.8$ ,  $a_{21} := -0.7$ ,  $a_{31} := 2d \cos(2\pi f_0)$ , and  $a_{32} := -d^2$  with  $d = 0.9$  and  $f_0 = 0.2$ , and where  $\{\varepsilon_{1,t}\}$ ,  $\{\varepsilon_{2,t}\}$ , and  $\{\varepsilon_{3,t}\}$  are mutually independent Gaussian white noise. By construction, the ordinary spectrum of  $\{\xi_{1,t}\}$  has a broad peak at  $\omega = 0$ , the ordinary spectrum of  $\{\xi_{2,t}\}$  has a broad peak at  $\omega = \pi$ , and the ordinary spectrum of  $\{\xi_{3,t}\}$  has a narrow peak at  $\omega = 2\pi \times 0.2$ .

Let  $\{z_t\}$  be a nonlinear mixture of  $\{\xi_{1,t}\}$  and  $\{\xi_{2,t}\}$  defined by

$$z_t := \psi_1(\xi_{1,t}) \times \xi_{1,t} + (1 - \psi_1(\xi_{1,t})) \times \xi_{2,t},$$

where  $\psi_1(y) := 0.9 \mathcal{I}(y < -0.8) + 0.2 \mathcal{I}(y > 0.8) + \{0.9 - (7/16)(y + 0.8)\} \mathcal{I}(|y| \leq 0.8)$ . Because  $\psi_1(y)$  equals 0.9 for  $y < -0.8$  and 0.2 for  $y > 0.8$ , the series  $\{z_t\}$  behaves very similarly to  $\{\xi_{1,t}\}$  at lower quantiles and somewhat similarly to  $\{\xi_{2,t}\}$  at higher quantiles. The final series  $\mathbf{y}_t := [y_{1,t}, y_{2,t}]^T$  is given by

$$\begin{cases} y_{1,t} := \psi_2(z_t) \times z_t + (1 - \psi_2(z_t)) \times \xi_{3,t}, \\ y_{2,t} := \xi_{3,t+10}, \end{cases} \quad (19)$$

where  $\psi_2(y) := 0.5 \mathcal{I}(y < -0.4) + \mathcal{I}(y > 0.4) + \{0.5 + (5/8)(y + 0.4)\} \mathcal{I}(|y| \leq 0.4)$ . Because  $\psi_2(y)$  equals 0.5 for  $y < -0.4$  and 1 for  $y > 0.4$ , the series  $\{y_{1,t}\}$  behaves similarly to  $\{z_t\}$  at higher quantiles and blends the characteristics of  $\{z_t\}$  and  $\{\xi_{3,t}\}$  at lower quantiles. The series  $\{y_{2,t}\}$  is a copy of  $\{\xi_{3,t}\}$  delayed by 10 units of time.

Figure 1 depicts the quantile spectrum of the process defined by (19). This is the ensemble mean of the quantile periodograms defined by (6) from 5000 Monte Carlo runs, computed at

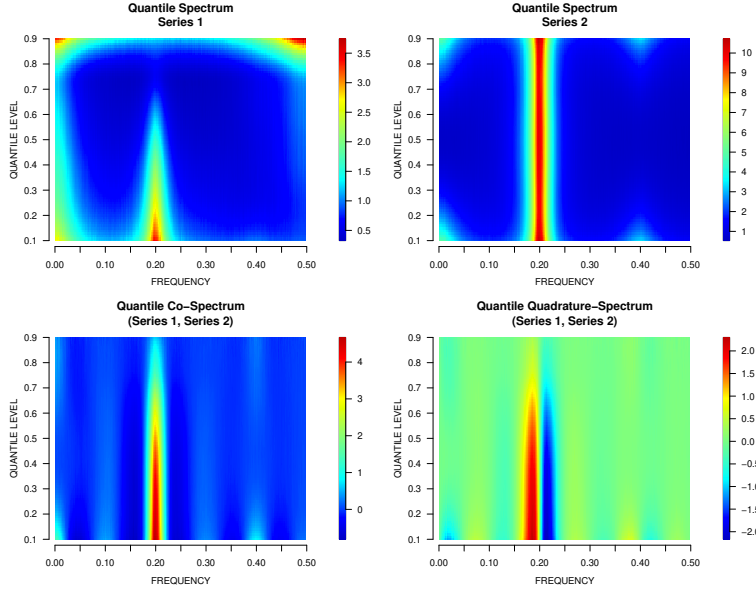


Figure 1: Quantile spectrum of the mixture process (19). Real and complex parts of the cross-spectrum (second row) are known as co-spectrum and quadrature-spectrum, respectively. All spectra are shown as functions of frequency variable  $f := \omega/(2\pi) \in (0, 0.5)$ .

$\omega_v = 2\pi v/n$  ( $v = 1, \dots, \lfloor (n-1)/2 \rfloor; n = 512$ ) and  $\alpha_\ell = 0.1 + 0.01(\ell - 1)$  ( $\ell = 1, \dots, 81$ ). Here, the quantile grid is chosen somewhat arbitrarily to exclude extreme quantiles due to their different statistical properties (Koenker 2005, p. 130; Davis and Mikosch 2009). As shown in Figure 1, the frequency-domain characteristics of the component series  $\{\xi_{1,t}\}$ ,  $\{\xi_{2,t}\}$ , and  $\{\xi_{3,t}\}$  are reflected as quantile-dependent patterns in the quantile spectrum of  $\{y_{1,t}\}$ . The quantile co-spectrum and quadrature-spectrum reveals a strong correlation between  $\{y_{1,t}\}$  and  $\{y_{2,t}\}$  in the lower and middle quantile region around frequency  $2\pi \times 0.2$ .

Figure 2 shows an example of the time series generated according to (19). Figure 3 depicts the corresponding QSER at quantile levels  $\alpha = 0.1, 0.5$ , and  $0.9$ . Figure 4 shows the spectral estimate obtained from this series by the AR estimator without quantile smoothing. This estimate is able to capture some key features of the underlying spectrum, including the spectral peak around frequency  $0.2 \times 2\pi$  and the dependency of its magnitude on quantile levels. However,

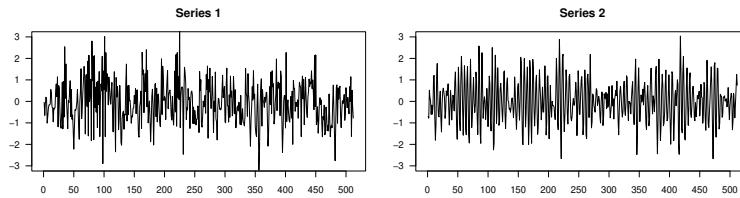


Figure 2: An example of simulated time series ( $n = 512$ ) according to (19).

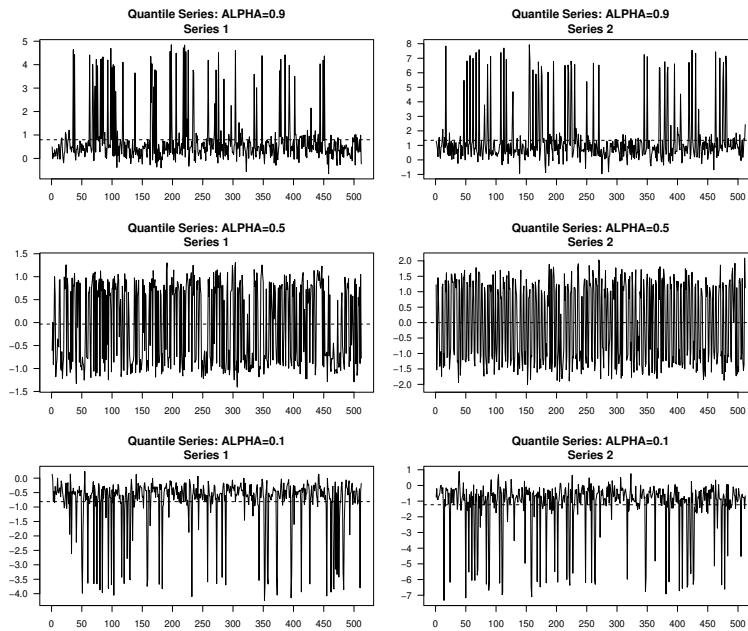


Figure 3: Quantile series obtained from the series shown in Figure 2 at  $\alpha = 0.9$  (first row),  $\alpha = 0.5$  (second row), and  $\alpha = 0.1$  (third row). Dashed horizontal line depicts the sample mean of quantile series which coincides with the sample quantile of the original series.

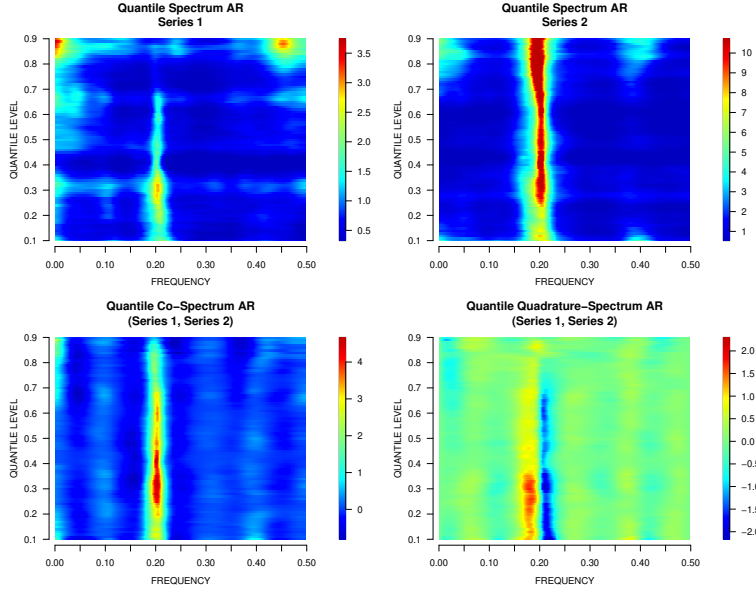


Figure 4: The AR estimate (without quantile smoothing) of the quantile spectrum shown in Figure 1 obtained from the series shown in Figure 2. (KLD = 0.183).

without quantile smoothing, this estimate remains noisy across quantiles.

To measure the accuracy of spectral estimation, we employ the Kullback-Leibler spectral divergence defined by

$$\text{KLD} := \frac{1}{L \lfloor (n-1)/2 \rfloor} \sum_{\ell=1}^L \sum_{v=1}^{\lfloor (n-1)/2 \rfloor} \left\{ \text{tr}(\hat{\mathbf{S}}(\omega_v, \alpha_\ell) \mathbf{S}^{-1}(\omega_v, \alpha_\ell)) - \log \frac{|\hat{\mathbf{S}}(\omega_v, \alpha_\ell)|}{|\mathbf{S}(\omega_v, \alpha_\ell)|} - m \right\}.$$

This is a nonnegative quantity which equals zero when  $\hat{\mathbf{S}}(\omega_v, \alpha_\ell) = \mathbf{S}(\omega_v, \alpha_\ell)$  for all  $v$  and  $\ell$ . The KLD is related to Whittle's likelihood for time series modeling (Whittle 1953) and has been used as the dissimilarity measure of ordinary spectra for time series clustering and classification (Kakizawa et al. 1998). For the AR estimate shown in Figure 4, we have  $\text{KLD} = 0.183$ .

Before presenting the SAR estimate, we would like to use Figure 5 to demonstrate the difficulty of selecting  $p$  and  $\lambda$  jointly using  $\text{tr}(\mathbf{H})$  as the effective degree of freedom. In this figure,  $\text{tr}(\mathbf{H})$  is plotted against the smoothing parameter  $\text{spar}$ , a reparameterized monotone function of  $\lambda$  (see Appendix I), for some fixed values of  $p$ . As expected for a meaningful degree-of-freedom measure, the trace decreases with  $\text{spar}$  for fixed  $p$  and increases with  $p$  for fixed  $\text{spar}$ . However,



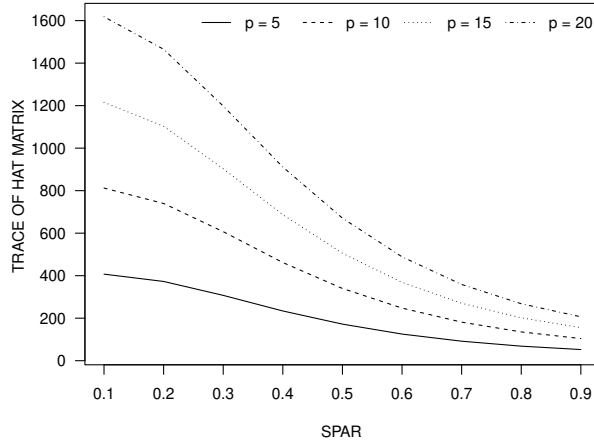


Figure 5: Illustration of  $\text{tr}(\mathbf{H})$  in the SAR problem (13) as a function of the smoothing parameter  $\text{spar}$  for different values of the order parameter  $p$ .

when considered jointly, the effect of a large  $p$  can be mitigated by the choice of a large  $\text{spar}$ , resulting in an unchanged value of  $\text{tr}(\mathbf{H})$ .

Returning to spectral estimation, Figure 6 shows the SAR estimate obtained from the series in Figure 2 with  $\text{spar}$  determined by the GCV in (17). This estimate exhibits remarkably improved smoothness across quantiles in comparison with the estimate shown in Figure 4. The improvement in appearance is reflected in the reduced KLD, which equals 0.100.

A more comprehensive comparison is presented in Table 1. This table contains the mean KLD of the SAR estimator computed from 1000 Monte Carlo runs with two sample sizes. The fixed value of  $\text{spar}$  corresponds to the minimizer of the mean KLD when  $p = 10$ , as shown in Figure 7. The order  $p = 10$  yields the best result against the other choices in Figure 7. This can be explained by the fact that  $\{y_{2,t}\}$  is a copy of  $\{\xi_{3,t}\}$  delayed by 10 units of time. According to Figure 7, there exists a range of choices for  $\text{spar}$  to yield an improved KLD for the SAR estimator over the AR estimator without quantile smoothing.

Besides the SAR estimator, Table 1 also contains the results from the AR and LW estimators with and without quantile smoothing. Two procedures are employed for quantile smoothing: the

Table 1: Mean KLD of Spectral Estimators for the Mixture Process (19)

$n$	SAR			AR		LW		
	GCV	Fixed spar	None	SPLINE	GAMM	None	SPLINE	GAMM
256	0.194	0.181	0.309	0.303	0.230	0.313	0.307	0.233
512	0.098	0.097	0.178	0.175	0.119	0.204	0.200	0.138

Results are based on 1000 Monte Carlo runs. Fixed spar: spar = 1 for  $n = 256$  and spar = 0.9 for  $n = 512$ .

SPLINE: `smooth.spline`. GAMM: `gamm` with correlated residuals. LW: lag-window estimator using Tukey-Hanning window with optimal bandwidth parameter ( $M = 24$  for  $n = 256$  and  $M = 30$  for  $n = 512$ ).

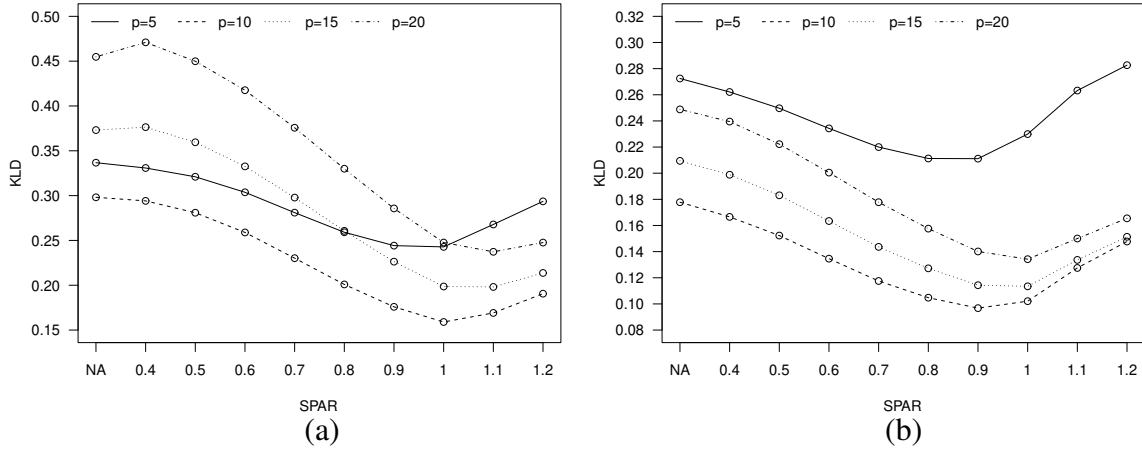


Figure 7: Mean KLD of the SAR estimator for the mixture process (19) with different choices of  $p$  and spar (spar = NA corresponds to the AR estimator without quantile smoothing). (a)  $n = 256$ . (b)  $n = 512$ . Results are based on 1000 Monte Carlo runs.

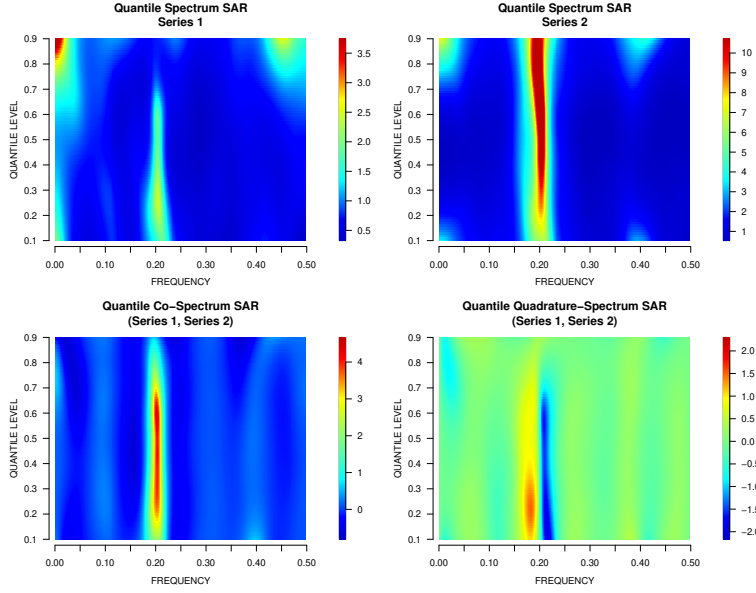


Figure 6: The SAR estimate of the quantile spectrum shown in Figure 1 from the series shown in Figure 2 with the smoothing parameter selected by GCV. (KLD = 0.100,  $spar = 0.904$ ).

R functions `smooth.spline` and `gamm`. While `smooth.spline` performs simple spline smoothing with GCV (Hastie and Tibshirani 1990, p. 27), `gamm` from the package ‘`mgcv`’ (Wood 2022) incorporates correlated residuals in the form a random effect with AR(1)-type correlation under the framework of generalized additive mixed-effect model. Table 1 shows the effectiveness of `gamm` in comparison with `smooth.spline` for quantile smoothing in both AR and LW estimators. These estimators are outperformed by the SAR estimator in Table 1.

A benefit of the SAR method is that the time-domain AR model with quantile-dependent functional coefficients can be used to perform Granger-causality analysis (Granger 1963; Lütkepohl 1993, p. 93) across quantiles. Details of this method can be found in Appendix II.

According to (19), the lagged series  $\{y_{2,t-\tau}\}$  is expected to exhibit a strong effect of Granger-causality for the series  $\{y_{1,t}\}$  at  $\tau = 10$ . This expectation is confirmed by the SAR-based Granger-causality analysis shown in Figure 8. The (1,2)-entry of  $\hat{\mathbf{A}}_{\tau}(\cdot)$  at lag  $\tau = 10$  as a function of  $\alpha$  resides entirely outside the 95% bootstrap confidence band constructed under the null hypothesis

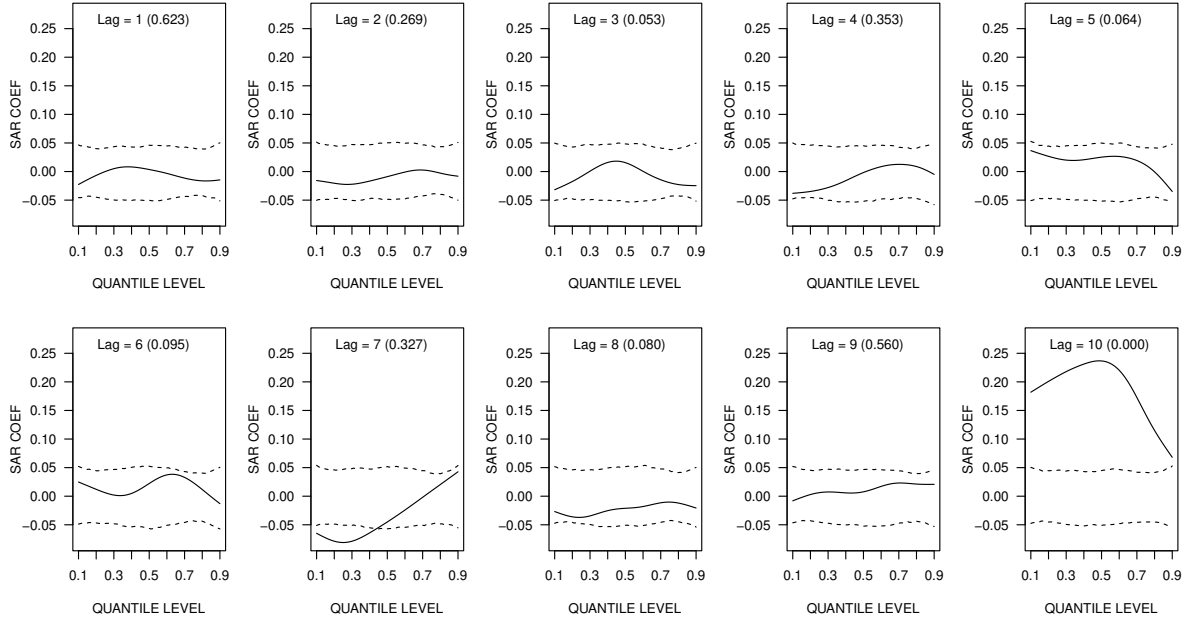


Figure 8: The (1,2)-entry of  $\hat{\mathbf{A}}_{\tau}(\cdot)$  at  $\tau = 1, \dots, 10$  for the series shown in Figure 2. Dashed lines depict the pointwise 95% bootstrap confidence band constructed from 1000 bootstrap samples under the null hypothesis of no Granger-causality. Numbers in parentheses are  $p$ -values of the bootstrap Wald statistic.

Table 2: Mean  $p$ -Values of Wald Test on (1,2)-Entry for the Mixture Process (19)

$\tau = 1$	$\tau = 2$	$\tau = 3$	$\tau = 4$	$\tau = 5$	$\tau = 6$	$\tau = 7$	$\tau = 8$	$\tau = 9$	$\tau = 10$	All $\tau$
0.329	0.331	0.340	0.293	0.172	0.310	0.188	0.184	0.199	0.000	0.000

Results are based on 1000 Monte Carlo run ( $n = 512$ ). The  $p$ -value in each run is computed from 1000 bootstrap samples.

of no Granger-causality. This entry at other lags lies mostly inside the respective confidence band. The statistical significance of this Granger-causality is manifested in the  $p$ -value of 0.000 for the corresponding bootstrap Wald statistic.

Table 2 contains the result of the bootstrap Wald test from 1000 Monte Carlo runs. As can be seen, this SAR-based test is able to detect the Granger-causality at  $\tau = 10$  with mean  $p$ -value equal to 0.000, whereas at the remaining lags the minimum mean  $p$ -value is 0.172.

## 6 Concluding Remarks

This paper proposes the spline autoregression (SAR) method for estimating the quantile spectrum introduced in Li (2012; 2014). The SAR spectral estimator is a bivariate function of frequency and quantile level. It is derived from an autoregression model where the coefficients are spline functions of the quantile level. This model is fitted by penalized least-squares to a set of quantile series (QSER) to produce a smoothing spline estimate. The simulation study validates the proposed method as an effective way of leveraging the smoothness of the quantile spectrum with respect to the quantile level to produce more accurate spectral estimates.

A key enabler of the SAR method is the creation of the QSER as the inverse Fourier transform of the quantile discrete Fourier transform (QDFT) computed by trigonometric quantile regression. It is conceivable that this machinery could be applied to the result of trigonometric  $M$ -regression where the objective function  $\rho_\alpha(\cdot)$  is replaced by another nonnegative function, as in Fajardo et al. (2018), which may be further indexed by a continuous parameter analogous to  $\alpha$ . Instead of periodogram smoothing, an AR or SAR model could be fitted to the resulting counterpart of the QSER to produce an estimate of the corresponding spectrum.

For conventional spectral analysis, the ARMA model is a more flexible extension of the AR model (Percival and Walden 1993; Stoica and Moses 1997), which is especially effective for time

series with deep spectral troughs. An interesting topic for future research is the employment of the ARMA model to estimate the quantile spectrum.

## References

- Baruník, J., and Kley, T. (2019). Quantile coherency: A general measure for dependence between cyclical economic variables. *Econometrics Journal*, 22, 131–152.
- Brockwell, P., and Davis, R. (1991). *Time Series: Theory and Methods*, 2nd edn. New York: Springer-Verlag.
- Chen, T., Sun, Y., and Li, T.-H. (2021). A semi-parametric estimation method for the quantile spectrum with an application to earthquake classification using convolutional neural network. *Computational Statistics and Data Analysis*, 154, 107069.
- Cheng, H., Wang, Y., Wang, Y., and Yang, T. (2022). Inferring causal interactions in financial markets using conditional Granger causality based on quantile regression. *Computational Economics*, 59, 719–748.
- Choi, B. (1993). Multivariate maximum entropy spectrum. *Journal of Multivariate Analysis*, 46, 56–60.
- Chuang, C.-C., Kuan, C.-M., and Lin, H.-Y. (2009). Causality in quantiles and dynamic stock return–volume relations. *Journal of Banking and Finance*, 33, 1351–1360.
- Davis, R., and Mikosch, T. (2009). The extremogram: A correlogram for extreme events. *Bernoulli*, 15, 977–1009.
- Dette, H., Hallin, M., Kley, T., and Volgushev, S. (2015). Of copulas, quantiles, ranks and spectra: an  $L_1$ -approach to spectral analysis. *Bernoulli*, 21, 781–831.
- Fajardo, H., Reisen, V., Lévy-Leduc, C., and Taqqu, M. (2018).  $M$ -periodogram for the analysis of long-range dependent time series. *Statistics*, 52, 665–683.
- Granger, C. (1969). Causal relations by econometric models and cross-spectral methods. *Econometrica*, 37, 424–438.
- Hagemann, A. (2013). Robust spectral analysis. arXiv:1111.1965.
- Hastie, T., and Tibshirani, R. (1990). *Generalized Additive Models*. Boca Raton, FL: CRC Press.
- Hong, Y. (2000). Generalized spectral tests for serial dependence. *Journal of the Royal Statistical Society Series B*, 62, 557–574.

- Jiménez-Varón, C., Sun, Y., and Li, T.-H. (2024). A semi-parametric estimation method for quantile coherence with an application to bivariate financial time series clustering. *Econometrics and Statistics*. <https://doi.org/10.1016/j.ecosta>
- Jordanger, L., and Tjøstheim, D. (2022). Nonlinear spectral analysis: a local Gaussian approach. *Journal of the American Statistical Association*, 117, 1010–1027.
- Jordanger, L., and Tjøstheim, D. (2023). Local Gaussian cross-spectrum analysis. *Econometrics*, 11, 1–27.
- Kakizawa, Y., Shumway, R., and Taniguchi, M. (1998). Discrimination and clustering for multivariate time series. *Journal of the American Statistical Association*, 93, 328–340.
- Kedem, B. (1986). Spectral analysis and discrimination by zero-crossings. *Proceedings of the IEEE*, 74, 1477–1493.
- Koenker, R. (2005). *Quantile Regression*. Cambridge, UK: Cambridge University Press.
- Li, T.-H. (2012). Quantile periodograms. *Journal of the American Statistical Association*, 107, 765–776.
- Li, T.-H. (2014). *Time Series with Mixed Spectra*. Boca Raton, FL: CRC Press.
- Li, T.-H. (2020). From zero crossings to quantile-frequency analysis of time series with an application to nondestructive evaluation. *Applied Stochastic Models for Business and Industry*, 36, 1111–1130.
- Li, T.-H. (2021). Quantile-frequency analysis and spectral measures for diagnostic checks of time series with nonlinear dynamics. *Journal of the Royal Statistical Society Series C*, 70, 270–290.
- Li, T.-H. (2022). Quantile Fourier transform, quantile series, and nonparametric estimation of quantile spectra. arXiv:2211.05844v1.
- Lim, Y., and Oh, H.-S. (2022). Quantile spectral analysis of long-memory processes. *Empirical Economics*, 62, 1245–1266.
- Lütkepohl, H. (1993). *Introduction to Multiple Time Series Analysis*, 2nd edn. New York: Springer-Verlag.
- Meziani, A., Medkour, T., and Djouani, K. (2020). Penalised quantile periodogram for spectral estimation. *Journal of Statistical Planning and Inference*, 207, 86–98.
- Parzen, E. (1982). Maximum entropy interpretation of autoregressive spectral densities. *Statistics & Probability Letters*, 1, 7–11.

- Percival, D., and Walden, A. (1993). *Spectral Analysis for Physical Applications*, Chap. 9. Cambridge, UK: Cambridge University Press.
- R Core Team (2024). R: A language and environment for statistical computing. R Foundation for Statistical Computing, Vienna, Austria. <https://www.R-project.org/>.
- Stoica, P., and Moses, R. (1997). *Introduction to Spectral Analysis*, Chap. 3. Upper Saddle River, NJ: Prentice Hall.
- Troster, V. (2018). Testing for Granger-causality in quantiles. *Econometric Reviews*, 37, 850–866.
- Whittle, P. (1953). Estimation and information in stationary time series. *Arkiv för Matematik*, 2, 423–434.
- Whittle, P. (1963). On the fitting of multivariate autoregressions, and the approximate canonical factorization of a spectral density matrix. *Biometrika*, 50, 129–134.
- Wiener, N., and Masani, P. (1957). The prediction theory of multivariate stochastic processes, I: The regularity condition. *Acta Mathematica*, 98, 111–150.
- Wiener, N., and Masani, P. (1958). The prediction theory of multivariate stochastic processes, II: The linear predictor. *Acta Mathematica*, 99, 93–137.
- Wood, S. (2022). Package ‘mgcv’. <https://cran.r-project.org/web/packages/mgcv/mgcv.pdf>.
- Wu, W. (2007). *M*-estimation of linear models with dependent errors. *Annals of Statistics*, 35, 495–521.



## Appendix I: Computation of Spline Autoregression

Recall that any  $\mathbf{A}_\tau(\cdot) \in \mathcal{F}_m$  can be written as  $\mathbf{A}_\tau(\cdot) = \mathbf{\Theta}_\tau \mathbf{\Phi}(\cdot)$ . Therefore, with  $\mathbf{\Theta}$ ,  $\mathbf{Y}_\ell$ , and  $\mathbf{Z}_\ell$  defined in Section 4, we have

$$\sum_{t=p+1}^n \left\| \mathbf{y}_t(\alpha_\ell) - \sum_{\tau=1}^p \mathbf{A}_\tau(\alpha_\ell) \mathbf{y}_{t-\tau}(\alpha_\ell) \right\|^2 = \|\mathbf{Y}_\ell - \mathbf{\Theta} \mathbf{Z}_\ell\|^2. \quad (20)$$

Due to the identity  $\text{vec}(\mathbf{\Theta} \mathbf{Z}_\ell) = (\mathbf{Z}_\ell^T \otimes \mathbf{I}_m) \text{vec}(\mathbf{\Theta})$ , we have

$$\|\mathbf{Y}_\ell - \mathbf{\Theta} \mathbf{Z}_\ell\|^2 = \|\mathbf{y}_\ell - \mathbf{X}_\ell \boldsymbol{\theta}\|^2 \quad (21)$$

where  $\boldsymbol{\theta} := \text{vec}(\mathbf{\Theta}) \in \mathbb{R}^{Km^2p}$ ,  $\mathbf{y}_\ell := \text{vec}(\mathbf{Y}_\ell) \in \mathbb{R}^{m(n-p)}$ , and  $\mathbf{X}_\ell := \mathbf{Z}_\ell^T \otimes \mathbf{I}_m \in \mathbb{R}^{(n-p) \times Km^2p}$ .

In addition, because  $[\mathbf{\Theta}_1 \ddot{\mathbf{\Phi}}(\alpha), \dots, \mathbf{\Theta}_p \ddot{\mathbf{\Phi}}(\alpha)] = \mathbf{\Theta} (\mathbf{I}_p \otimes \ddot{\mathbf{\Phi}}(\alpha))$  and  $\text{vec}(\mathbf{\Theta} (\mathbf{I}_p \otimes \ddot{\mathbf{\Phi}}(\alpha))) = ((\mathbf{I}_p \otimes \ddot{\mathbf{\Phi}}(\alpha))^T \otimes \mathbf{I}_m) \text{vec}(\mathbf{\Theta})$ , we have

$$\sum_{\tau=1}^p \|\mathbf{\Theta}_\tau \ddot{\mathbf{\Phi}}(\alpha)\|^2 = \|\mathbf{\Theta} (\mathbf{I}_p \otimes \ddot{\mathbf{\Phi}}(\alpha))\|^2 = \|(\mathbf{I}_p \otimes \ddot{\mathbf{\Phi}}^T(\alpha) \otimes \mathbf{I}_m) \boldsymbol{\theta}\|^2. \quad (22)$$

Substituting (20)–(22) in (13) leads to the following reformulations of the SAR problem:

$$\hat{\boldsymbol{\Theta}} := \underset{\boldsymbol{\Theta} \in \mathbb{R}^{m \times Lmp}}{\text{argmin}} \left\{ \sum_{\ell=1}^L \|\mathbf{Y}_\ell - \mathbf{\Theta} \mathbf{Z}_\ell\|^2 + (n-p)\lambda \int_{\underline{\alpha}}^{\bar{\alpha}} \|\mathbf{\Theta} (\mathbf{I}_p \otimes \ddot{\mathbf{\Phi}}(\alpha))\|^2 d\alpha \right\}, \quad (23)$$

$$\hat{\boldsymbol{\theta}} := \underset{\boldsymbol{\theta} \in \mathbb{R}^{Lm^2p}}{\text{argmin}} \left\{ \sum_{\ell=1}^L \|\mathbf{y}_\ell - \mathbf{X}_\ell \boldsymbol{\theta}\|^2 + (n-p)\lambda \int_{\underline{\alpha}}^{\bar{\alpha}} \|(\mathbf{I}_p \otimes \ddot{\mathbf{\Phi}}^T(\alpha) \otimes \mathbf{I}_m) \boldsymbol{\theta}\|^2 d\alpha \right\}. \quad (24)$$

The normal equations of (23) take the form

$$\boldsymbol{\Theta} \left( \sum_{\ell=1}^L \mathbf{Z}_\ell \mathbf{Z}_\ell^T + (n-p)\lambda \mathbf{D} \right) = \sum_{\ell=1}^L \mathbf{Y}_\ell \mathbf{Z}_\ell^T,$$

where  $\mathbf{D} := \mathbf{I}_p \otimes \int_{\underline{\alpha}}^{\bar{\alpha}} \ddot{\mathbf{\Phi}}(\alpha) \ddot{\mathbf{\Phi}}^T(\alpha) d\alpha$ . The normal equations of (24) take the form

$$\left( \sum_{\ell=1}^L \mathbf{X}_\ell^T \mathbf{X}_\ell + (n-p)\lambda (\mathbf{D} \otimes \mathbf{I}_m) \right) \boldsymbol{\theta} = \sum_{\ell=1}^L \mathbf{X}_\ell^T \mathbf{y}_\ell.$$

Therefore, the SAR solution can be expressed as

$$\hat{\boldsymbol{\Theta}} = \left( \sum_{\ell=1}^L \mathbf{Y}_\ell \mathbf{Z}_\ell^T \right) \left( \sum_{\ell=1}^L \mathbf{Z}_\ell \mathbf{Z}_\ell^T + (n-p)\lambda \mathbf{D} \right)^{-1}, \quad (25)$$

$$\hat{\boldsymbol{\theta}} = \left( \sum_{\ell=1}^L \mathbf{X}_\ell^T \mathbf{X}_\ell + (n-p)\lambda (\mathbf{D} \otimes \mathbf{I}_m) \right)^{-1} \left( \sum_{\ell=1}^L \mathbf{X}_\ell^T \mathbf{y}_\ell \right). \quad (26)$$

Note that (25) is more efficient computationally when  $m$  is large because it requires the inversion of a  $Kmp$ -by- $Kmp$  matrix, whereas (26) requires the inversion of an  $Km^2p$ -by- $Km^2p$  matrix.

The hat (or smoothing) matrix associated with (24) is given by

$$\mathbf{H} := \mathbf{X}_0 \left[ \sum_{\ell=1}^L \mathbf{X}_\ell^T \mathbf{X}_\ell + (n-p)\lambda(\mathbf{D} \otimes \mathbf{I}_m) \right]^{-1} \mathbf{X}_0^T,$$

where  $\mathbf{X}_0 := [\mathbf{X}_1^T, \dots, \mathbf{X}_L^T]^T$ . Therefore,

$$\begin{aligned} \text{tr}(\mathbf{H}) &= \sum_{\ell'=1}^L \text{tr} \left( \mathbf{X}_{\ell'} \left[ \sum_{\ell=1}^L \mathbf{X}_\ell^T \mathbf{X}_\ell + (n-p)\lambda(\mathbf{D} \otimes \mathbf{I}_m) \right]^{-1} \mathbf{X}_{\ell'}^T \right) \\ &= \sum_{\ell'=1}^L \text{tr} \left( (\mathbf{Z}_{\ell'}^T \otimes \mathbf{I}_m) \left[ \left( \sum_{\ell=1}^L \mathbf{Z}_\ell \mathbf{Z}_\ell^T + (n-p)\lambda \mathbf{D} \right) \otimes \mathbf{I}_m \right]^{-1} (\mathbf{Z}_{\ell'}^T \otimes \mathbf{I}_m)^T \right) \\ &= \sum_{\ell'=1}^L \text{tr} \left( \mathbf{Z}_{\ell'}^T \left[ \sum_{\ell=1}^L \mathbf{Z}_\ell \mathbf{Z}_\ell^T + (n-p)\lambda \mathbf{D} \right]^{-1} \mathbf{Z}_{\ell'} \otimes \mathbf{I}_m \right) \\ &= \sum_{\ell'=1}^L \text{tr} \left( \mathbf{Z}_{\ell'}^T \left[ \sum_{\ell=1}^L \mathbf{Z}_\ell \mathbf{Z}_\ell^T + (n-p)\lambda \mathbf{D} \right]^{-1} \mathbf{Z}_{\ell'} \right) \times m. \end{aligned}$$

The GCV criterion in (17) can be expressed as

$$\text{GCV}(\lambda) = \frac{(L(n-p))^{-1} \sum_{\ell=1}^L \|\mathbf{Y}_\ell - \hat{\boldsymbol{\Theta}} \mathbf{Z}_\ell\|^2}{\{1 - (L(n-p))^{-1} \text{tr}(\mathbf{H})\}^2}.$$

By following the convention in `smooth.spline`, the smoothing parameter  $\lambda$  can be reparameterized by `spar` such that  $\lambda = r \times 256^{3 \times \text{spar} - 1}$ , with  $r := (n-p)^{-1} \sum_{\ell=1}^L \text{tr}(\mathbf{Z}_\ell \mathbf{Z}_\ell^T) / \text{tr}(\mathbf{D})$ .

## Appendix II: Granger-Causality Analysis

We extend the concept of Granger-causality for ordinary AR models (Granger 1969; Lükepohl 1993, Section 2.3) to the AR model with functional coefficients in (13) for the QSER. We say that  $\{y_{j',t}\}$  is Granger-causal for  $\{y_{j,t}\}$  at quantile level  $\alpha$  if the  $(j, j')$ -entry of  $\mathbf{A}_\tau(\alpha)$  in (13) is nonzero for some  $\tau \in \{1, \dots, p\}$ . This causality is related but not identical to the so-called Granger-causality in quantiles (Chuang et al. 2009; Troster 2018; Cheng et al. 2022). The latter

is defined in terms of quantile regression of the original series. The SAR-based Granger-causality is based on least-squares regression of the QSER.

Given the estimates  $\{\hat{\mathbf{A}}_\tau(\cdot) : \tau = 1, \dots, p\}$  from a data record  $\{\mathbf{y}_t : t = 1, \dots, n\}$ , one can detect the SAR-based Granger-causality by a bootstrap procedure under the assumption that  $\{\mathbf{y}_t(\alpha)\}$  is an AR process with coefficients  $\{\mathbf{A}_\tau(\alpha) : \tau = 1, \dots, p\}$  and the null hypothesis that

$$H_0 : \text{the } (j, j')\text{-entry of } \mathbf{A}_\tau(\alpha) \text{ equals zero for all } \tau \text{ and } \alpha. \quad (27)$$

Specifically, this bootstrap procedure comprises the following steps.

(a) Let  $\{\boldsymbol{\varepsilon}_t(\alpha_\ell) : t = 1, \dots, n\}$  be the residual series from fitting an AR( $p$ ) model to  $\{\mathbf{y}_t(\alpha_\ell) : t = 1, \dots, n\}$ . Generate  $\{\boldsymbol{\varepsilon}_t^{(b)}(\alpha_\ell) : t = 1, \dots, n_B\}$  ( $b = 1, \dots, B; n_B \gg n$ ) by sampling the time index  $\{1, \dots, n\}$  with replacement and rearranging the residuals accordingly.

(b) Let  $\mathbf{A}_\tau^{(0)}(\alpha_\ell)$  be the same as  $\hat{\mathbf{A}}_\tau(\alpha_\ell)$  except that the  $(j, j')$ -entry is set to zero for all  $\tau$  and  $\alpha_\ell$ . Generate  $\{\mathbf{y}_t^{(b)}(\alpha_\ell) : t = 1, \dots, n\}$  ( $b = 1, \dots, B; \ell = 1, \dots, L$ ) according to

$$\mathbf{y}_t^{(b)}(\alpha_\ell) = \sum_{\tau=1}^p \mathbf{A}_\tau(\alpha_\ell) \mathbf{y}_{t-\tau}^{(b)}(\alpha_\ell) + \boldsymbol{\varepsilon}_{n_B-n+t}^{(b)}(\alpha_\ell) \quad (t = -n_B + n + 1, \dots, n) \quad (28)$$

with  $\mathbf{y}_t^{(b)}(\alpha_\ell) := 0$  for  $t = -n_B + n + 1 - p, \dots, -n_B + n$ . The first  $n_B - n$  values from this recursion are discarded to minimize the effect of initial values.

(c) Solve the SAR problem (13) with  $\{\mathbf{y}_t^{(b)}(\alpha_\ell)\}$  in place of  $\{\mathbf{y}_t(\alpha_\ell)\}$  to obtain  $\{\hat{\mathbf{A}}_\tau^{(b)}(\cdot) : \tau = 1, \dots, p\}$  ( $b = 1, \dots, B$ ). From these samples, construct a pointwise bootstrap confidence band for the  $(j, j')$ -entry of  $\hat{\mathbf{A}}_\tau(\alpha)$  as a function of  $\alpha$  for each  $\tau$ , and compute the  $p$ -value of the bootstrap Wald statistic (Lükepohl 1993, Section 3.6)

$$W := \hat{\mathbf{a}}^T \boldsymbol{\Sigma}_B^\dagger \hat{\mathbf{a}},$$

where  $\hat{\mathbf{a}}$  is the vector formed by the  $(j, j')$ -entry of  $\hat{\mathbf{A}}_\tau(\alpha_\ell)$  ( $\tau = 1, \dots, p; \ell = 1, \dots, L$ ) and  $\boldsymbol{\Sigma}_B^\dagger$  is the generalized inverse of the sample covariance matrix of the vectors formed by the  $(j, j')$ -entry of  $\hat{\mathbf{A}}_\tau^{(b)}(\alpha_\ell)$  ( $\tau = 1, \dots, p; \ell = 1, \dots, L$ ) for  $b = 1, \dots, B$ .

## Appendix III: Additional Simulation Results

Consider the ARMA process  $\mathbf{y}_t := [y_{1,t}, y_{2,t}]^T$  defined by

$$\mathbf{y}_t - \mathbf{A}_1 \mathbf{y}_{t-1} - \mathbf{A}_2 \mathbf{y}_{t-2} = \boldsymbol{\varepsilon}_t + \mathbf{B} \boldsymbol{\varepsilon}_{t-1}, \quad \{\boldsymbol{\varepsilon}_t\} \sim \text{IID } \mathcal{N}(\mathbf{0}, \boldsymbol{\Sigma}), \quad (29)$$

where

$$\mathbf{A}_1 := \begin{bmatrix} 0.816 & 1.246 \\ 0.558 & 1.107 \end{bmatrix}, \quad \mathbf{A}_2 := \begin{bmatrix} 0.643 & 1.184 \\ 0.307 & 0.203 \end{bmatrix},$$

$$\mathbf{B} := \begin{bmatrix} 0 & 2.496 \\ 0.4 & 0 \end{bmatrix}, \quad \boldsymbol{\Sigma} := \begin{bmatrix} 0.04 & -0.02 \\ -0.02 & 0.02 \end{bmatrix}.$$

Figure 9 depicts the quantile spectrum of this process.

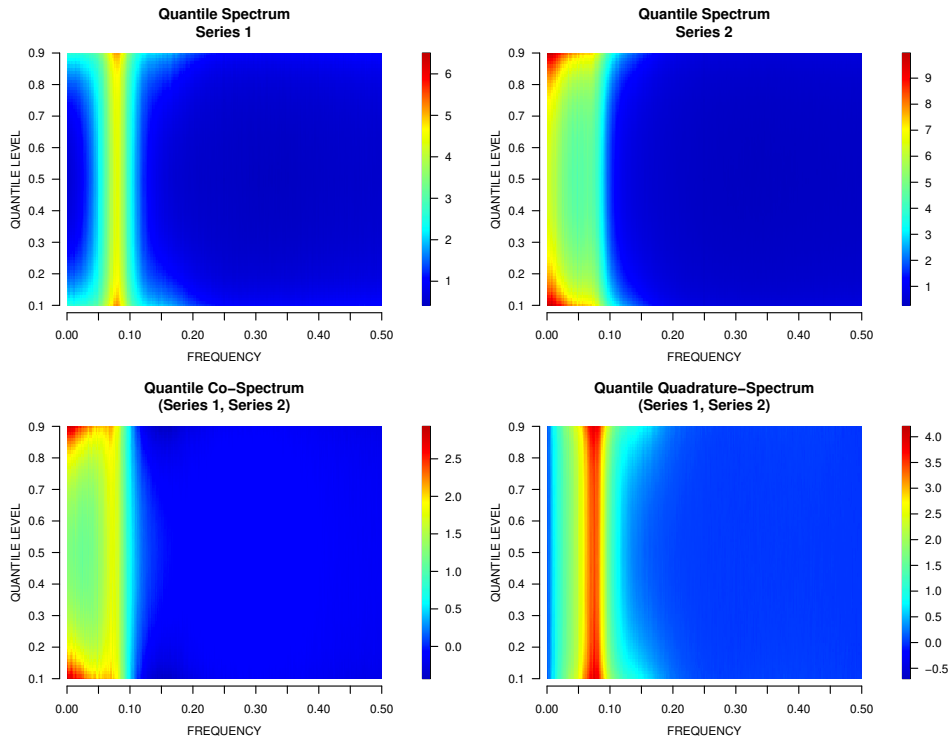


Figure 9: Quantile spectrum of the ARMA process (29).

Table 3: Mean KLD of Spectral Estimators for the ARMA Process (29)

$n$	SAR			AR		LW		
	GCV	Fixed spar	None	SPLINE	GAMM	None	SPLINE	GAMM
256	0.150	0.110	0.250	0.246	0.149	0.289	0.263	0.171
512	0.083	0.068	0.170	0.167	0.106	0.182	0.179	0.106

Results are based on 1000 Monte Carlo runs. Fixed spar: spar = 1 for  $n = 256$  and spar = 0.9 for  $n = 512$ .

SPLINE: `smooth.spline`. GAMM: `gamm` with correlated residuals. LW: lag-window estimator using Tukey-Hanning window with optimal bandwidth parameter  $M = 14$  for  $n = 256$  and  $M = 17$  for  $n = 512$ .

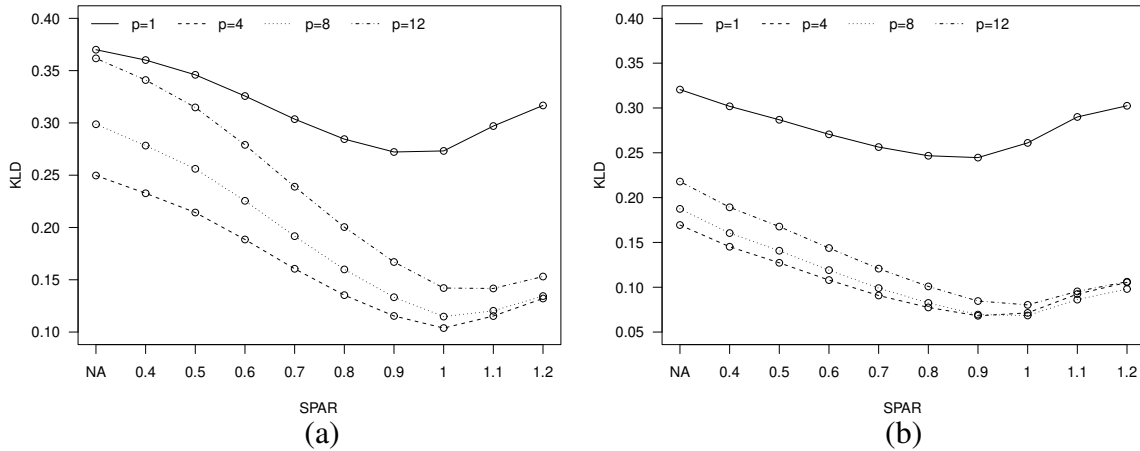


Figure 10: Mean KLD of the SAR estimator for the ARMA process (29) with different choices of  $p$  and spar (spar = NA corresponds to the AR estimator without quantile smoothing). (a)  $n = 256$ . (b)  $n = 512$ . Results are based on 1000 Monte Carlo runs

The results of spectral estimation for this process are shown in Table 3 and Figure 10. As can be seen in Table 3, the SAR estimator outperforms the AR and LW estimators with or without quantile smoothing. The mean KLD of the SAR estimator with the smoothing parameter selected by GCV is reasonably close to the best values achieved with fixed spar (Figure 10). These

findings are similar to the findings in Section 4 for the mixture process (19).

The results of SAR-based Granger-causality analysis for the ARMA process in (29) are shown in Figure 11 and Table 4. These results confirm the existence of Granger-causality of series 2 for series 1 as expected from (29). The effect of this causality is largely confined to  $\tau = 1$  and  $\tau = 4$ . It is stronger in the middle quantile region than in the tail regions.

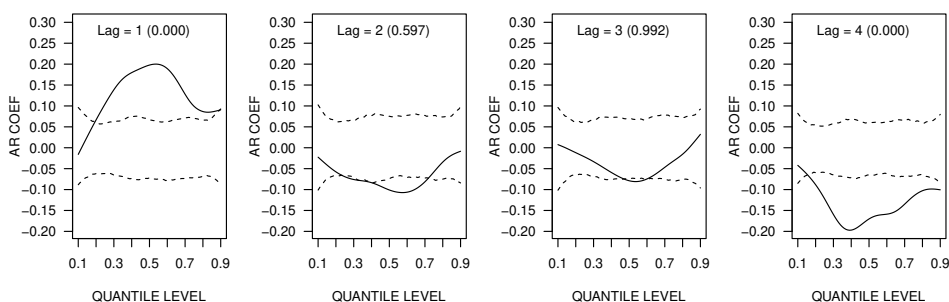


Figure 11: The (1,2)-entry of  $\hat{\mathbf{A}}_{\tau}(\cdot)$  at  $\tau = 1, \dots, 4$  for a series generated from the ARMA process in (29) with  $n = 512$ . Dashed lines depict the pointwise 95% bootstrap confidence band constructed from 1000 bootstrap samples under the hypothesis of no causality. Numbers in parentheses are  $p$ -values of the bootstrap Wald statistic.

Table 4: Mean  $p$ -Values of Wald Test on (1,2)-Entry for the ARMA Process (29)

$\tau = 1$	$\tau = 2$	$\tau = 3$	$\tau = 4$	All $\tau$
0.001	0.601	0.453	0.128	0.000

Results are based on 1000 Monte Carlo run ( $n = 512$ ). The  $p$ -value in each run is computed from 1000 bootstrap samples.

## Appendix IV: R Functions

The following functions in the R package ‘qfa’ (version  $\geq 3.0$ ) are implementations of the SAR method for quantile spectral estimation and Granger-causality analysis. The package is available for installation at [cran.r-project.org](http://cran.r-project.org) and [github.com/th12019/QFA](https://github.com/th12019/QFA).

- `qdft`: a function that computes the QDFT at a given sequence of quantile levels from a (univariate or multivariate) time series.
- `qper`: a function that computes the quantile periodogram at a given sequence of quantile levels from a time series or the QDFT.
- `qser`: a function that computes the QSER at a given sequence of quantile levels from a time series or the QDFT.
- `qacf`: a function that computes the QACF at a given sequence of quantile levels from a time series or the QDFT.
- `qspec.ar`: a function that computes the AR spectral estimate at a given sequence of quantile levels with or without subsequent quantile smoothing from a time series or the QSER.
- `qspec.sar`: a function that fits the SAR spectral estimate at a given sequence of quantile levels with or without subsequent quantile smoothing from a time series or the QSER.
- `qspec.lw`: a function that computes the LW spectral estimate at a given sequence of quantile levels with or without quantile smoothing from a time series or the QACF.
- `qfa.plot`: a function that produces an image plot for a real-valued spectrum as a function of frequency and quantile level

- `qkl.divergence`: a function that computes the Kullback-Leibler divergence (KLD) of a spectral estimate against the true spectrum.
- `sar.gc.coef`: a function that extracts the functional AR coefficients of the SAR model produced by `qspec.sar`.
- `sar.gc.bootstrap`: a function that generates bootstrap samples of functional AR coefficients from the SAR model produced by `qspec.sar` for Granger-causality analysis.
- `sar.gc.test`: a function that computes the bootstrap Wald statistic and its  $p$ -value for Granger-causality, together with the 95% confidence band, from the functional AR coefficients produced by `sar.gc.coef` and the corresponding bootstrap samples produced by `sar.gc.bootstrap`.